Supplemental figures (1-9)

Gu et al.

"ADF/Cofilin-Mediated Actin Dynamics Regulate AMPA Receptor Trafficking during Synaptic Plasticity"

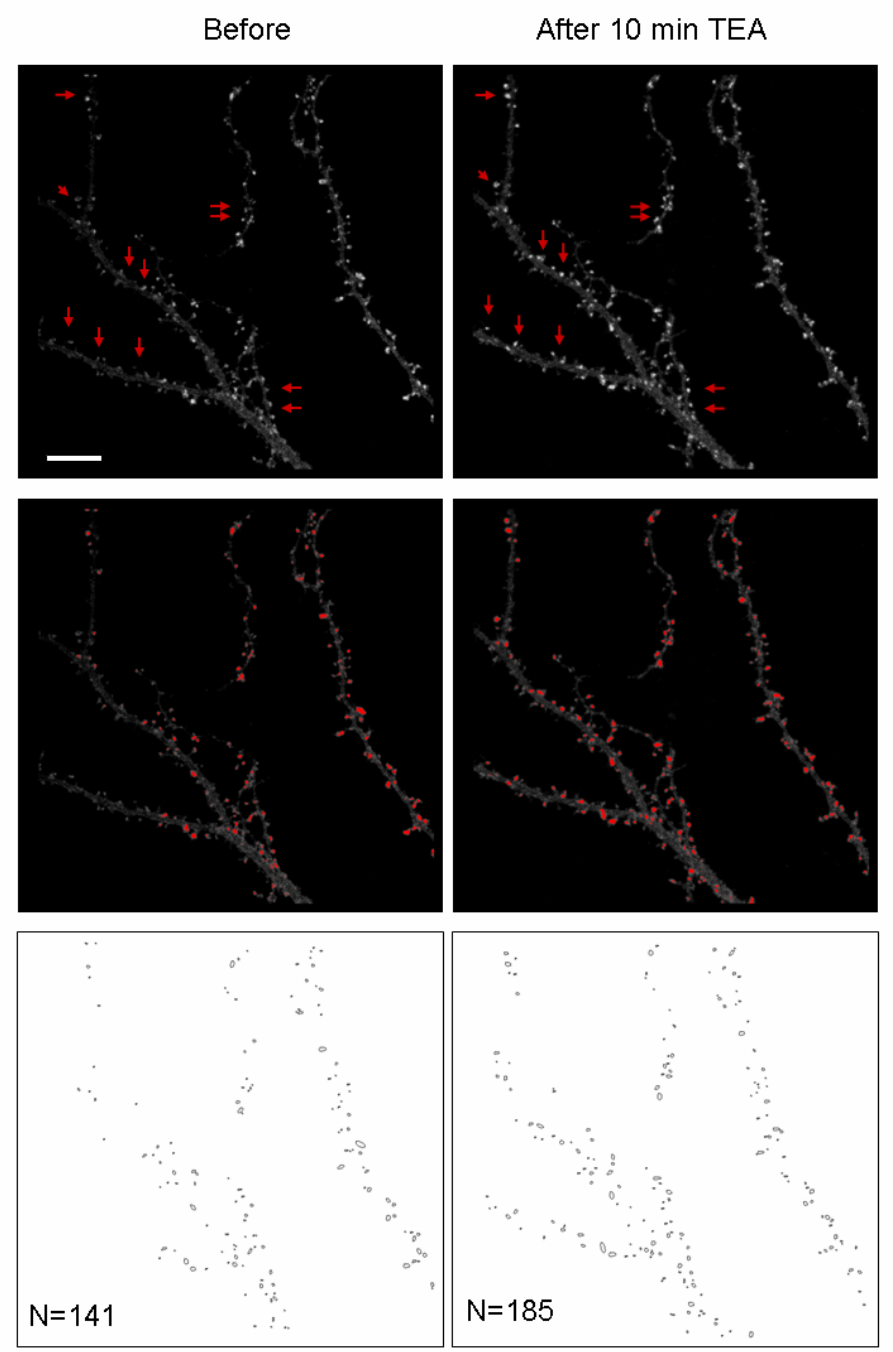

Supplemental figure 1. The quantification method to determine the number of spines with SEP-GluR1 fluorescence before and after cLTP induction. Confocal z-stacks of the dendritic region before and after TEA treatment were projected as 2-D images using by maximum intensity. ImageJ (NIH) was used for quantitative

analysis of spines with strong SEP-GluR1 fluorescence. Here, a fluorescent intensity threshold was set to select the spines with bright SEP-GluR1 signals while discriminating the dendritic shaft and those spines with weak SEP-GluR1 signals. The same threshold is applied to the image after TEA treatment. Spines that are selected by this threshold (in red color) are then counted using the object analysis function (see the bottom row of the images). Scale bar: 10 μm.

.

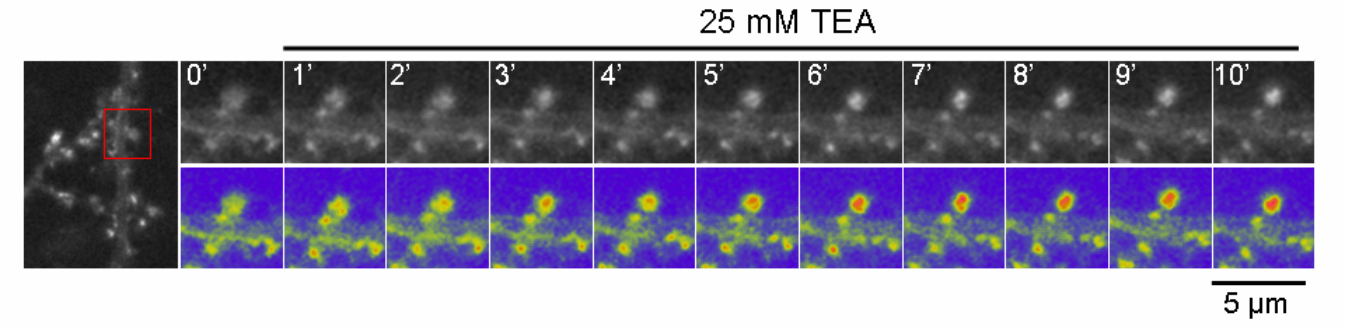

Supplemental figure 2. Fast time-lapse imaging on the rapid insertion of SEP-GluR1 to the spine surface. The time-lapse sequence was acquired at one frame every minute using a CCD-based wide-field fluorescence microscopy. A 100X/1.3 objective was used for imaging. The first panel shows a dendritic region of a hippocampal neuron expressing SEP-GluR1. The region enclosed by the red box is shown in the time sequence. To better depict the changes in SEP-GluR1 fluorescence, the same sequence was pseudocolor-coded and shown together with the grayscale sequence. Numbers indicate minutes after the onset of TEA treatment (25 mM). One can see that the spine increase in SEP-GluR1 fluorescence occurred before 6 min after TEA onset. The grayscale sequence also shows that the spine did not exhibit much change in size.

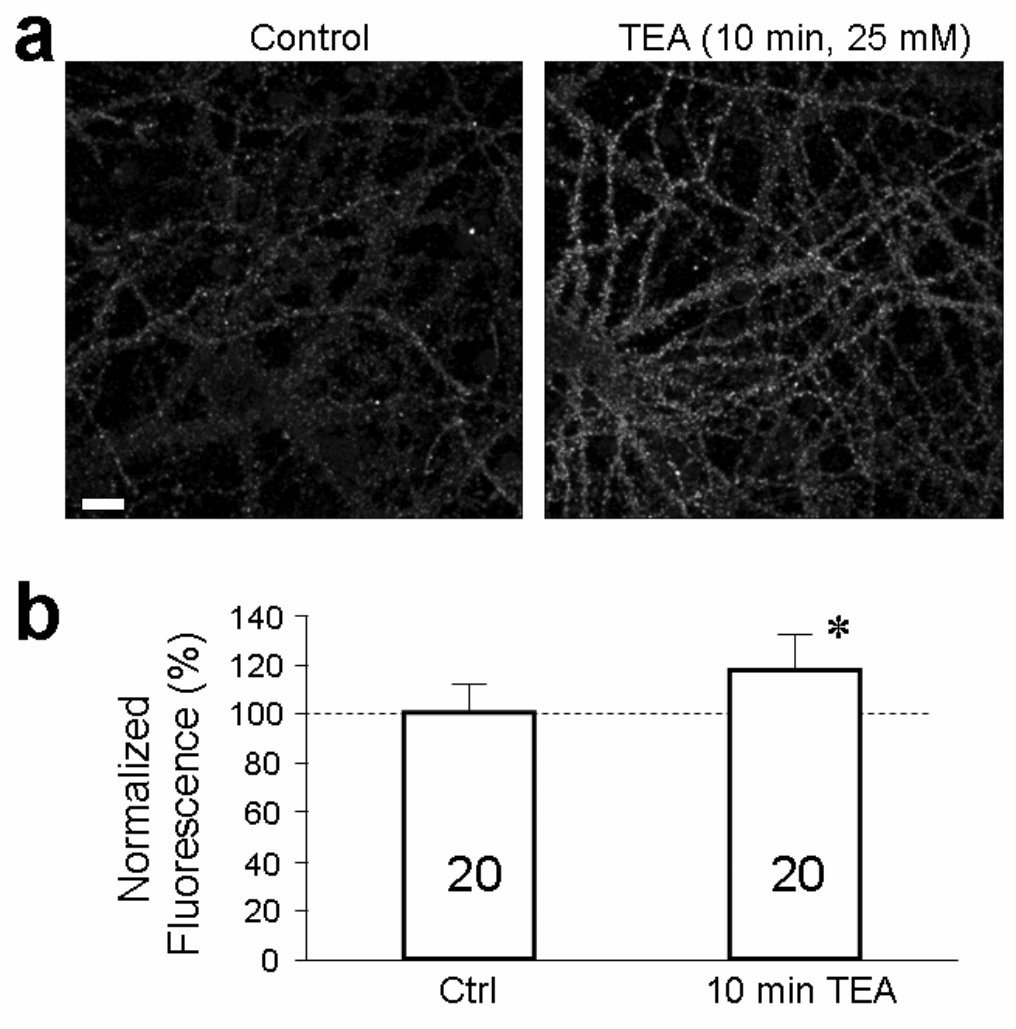

Supplemental figure 3. Immunostaining of surface GluR1 on hippocampal neurons before and after cLTP induction by TEA. (**a**) Representative images of surface GluR1 staining on hippocampal cultures with or without TEA treatment. (**b**) Normalized fluorescence quantification of the staining for cells with and without TEA treatment. Asterisk: $p<0.05$ when compared to the control. The numbers of cells examined are shown in the bars.

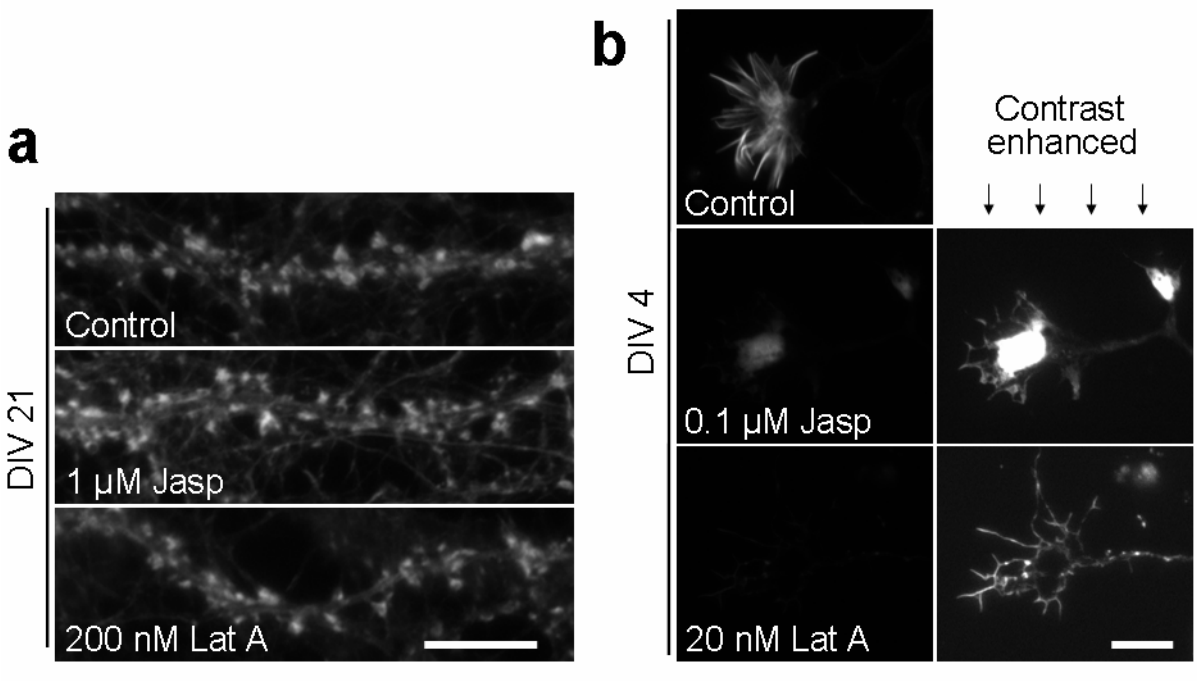

Supplemental figure 4. Effects of actin drugs on F-actin structures in different parts of the neurons. (**a**) Representative images of the dendritic spines labeled by a low concentration of rhodamine-phalloidin without and with either Jasplakinolide (1 µM) or Latrunculin A (200 nM). These two actin drugs appear to not grossly affect the spine morphology and the underlying actin structure. (**b**) Representative images of phalloidin staining showing growth cones of young neurons (DIV4) treated with Jasplakinolide or Latrunculin A. Unlike the spines, the growth cones of these young neurons appear to be quite sensitive to these actin drugs and showed marked disruption after treatment (20 min). Scale bars: 10 µm.

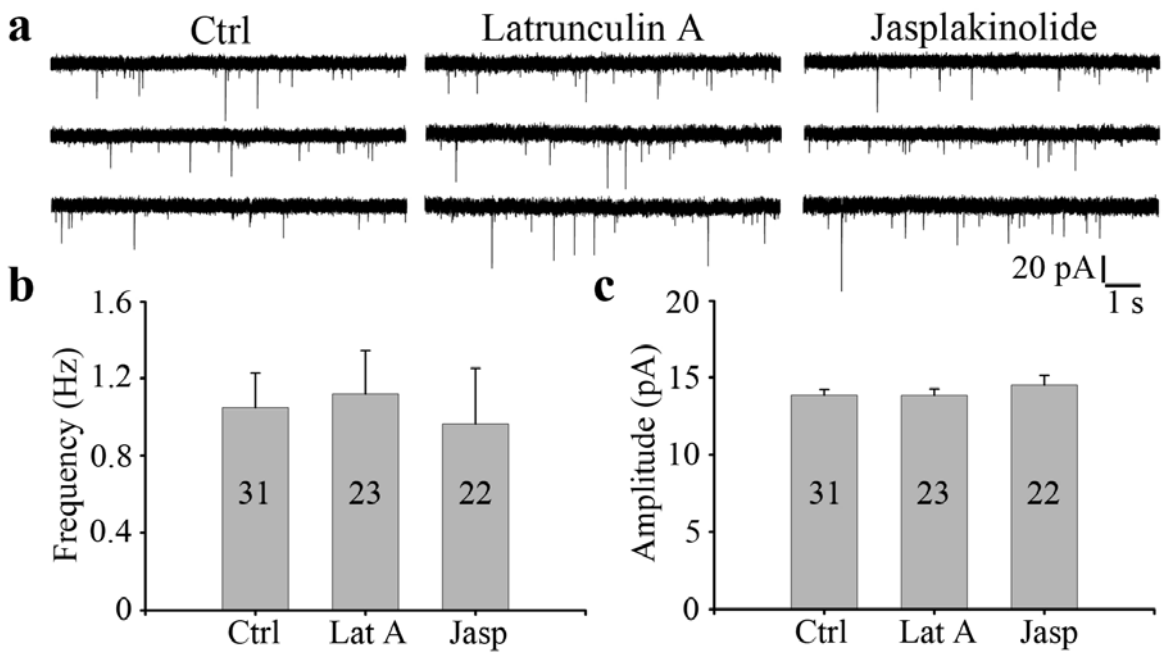

Supplemental figure 5. Basal synaptic transmission is not affected by Latrunculin A or Jasplakinolide treatment. (**a**) Representative traces of mEPSCs from control neurons and neurons after 20 min treatment with either latrunculin A (Lat A, 20 nM) or jasplakinolide (Jasp, 1 µM). (**b**) When compared with control, the mEPSC frequency showed no significant change after either Lat A ($p>0.8$, Student's *t*-test) or Jasp ($p>0.8$) treatment. (**c**) The mEPSC amplitude also showed no significant change after either Lat A ($p>0.9$) or Jasp ($p>0.3$) treatment. The number of neurons recorded in each group is shown with each bar.

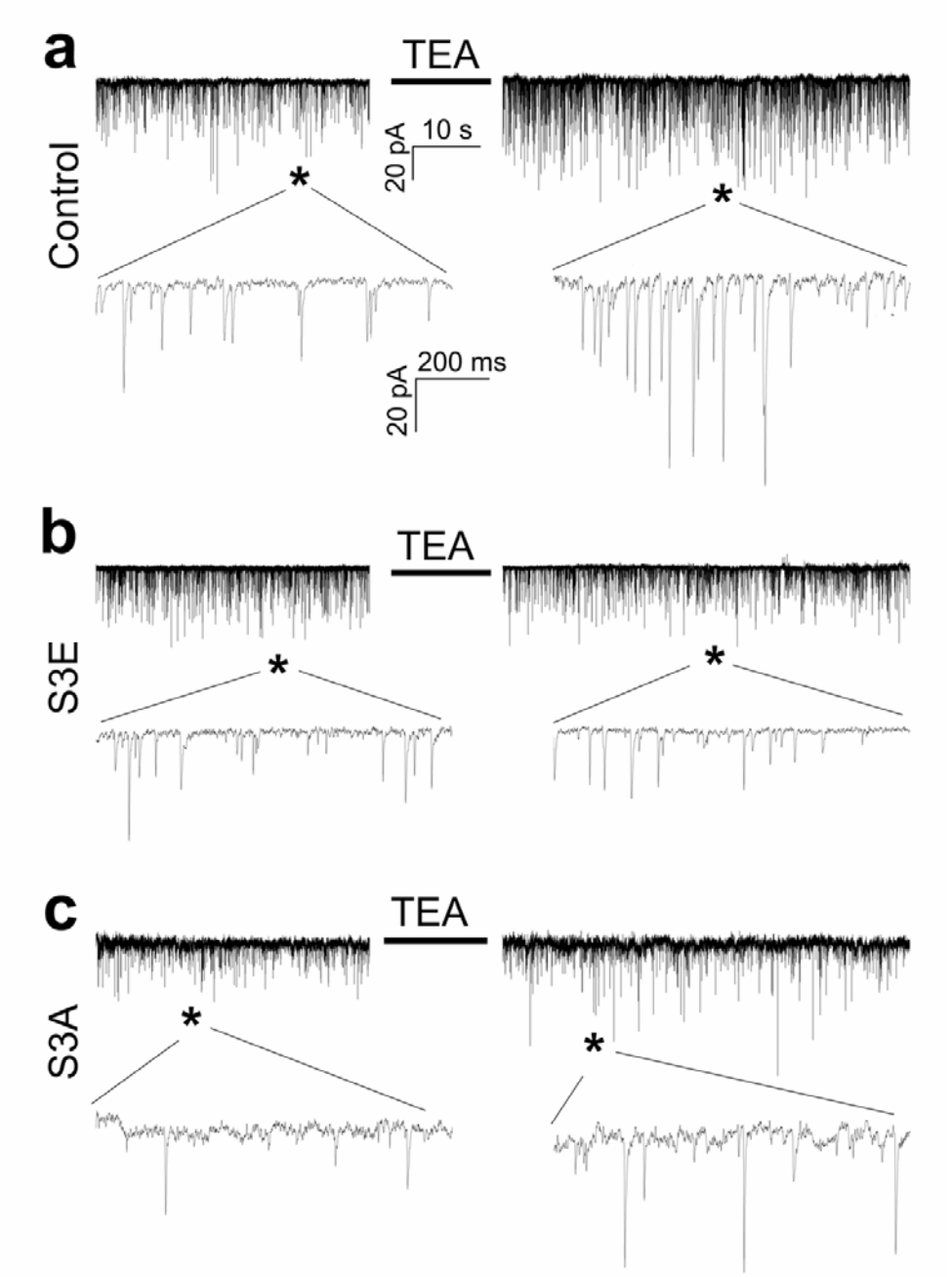

Supplemental figure 6. Effects of cofilin 3A and 3E on mEPSCs of hippocampal synapses. Sample traces of mEPSCs from our preliminary recordings from DIV21 control (a) neurons expressing cofilin S3E (b) and S3A (c) mutants before and after 10 min exposure to 25 mM TEA. The whole cell patch-clamp recordings were performed on the same neurons before and after 10 min TEA treatment, with the membrane voltage clamped at -70 mV and TTX in bath. 10 min TEA treatment was done in the absence of voltage clamp and TTX. No significant changes were observed with the basal activities as shown by the control period of recordings. 3E, but not 3A, appears to abolish the increase in the mEPSC frequency. About three cells per condition have been recorded, all showing the same trends.

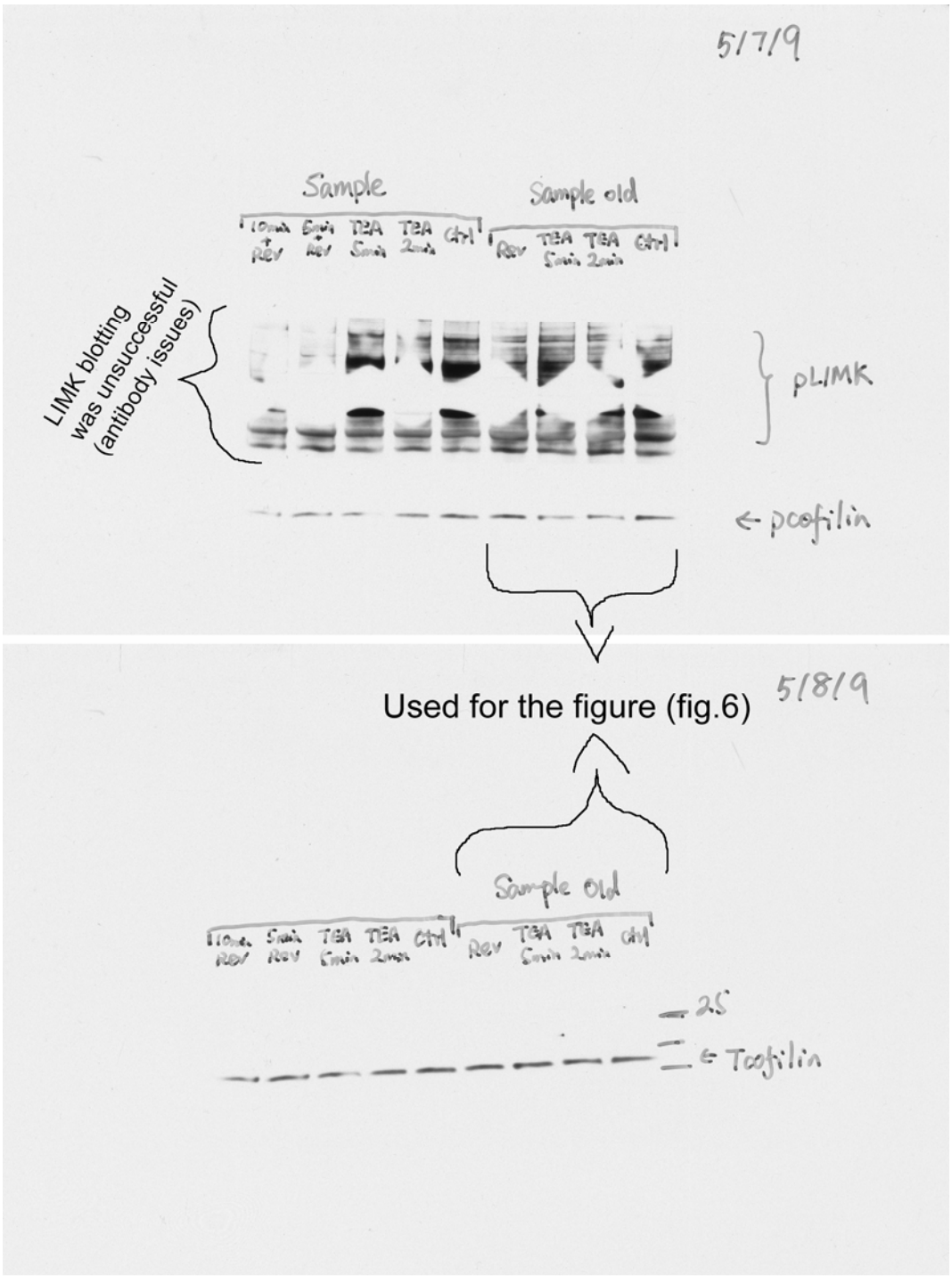

Supplemental figure 7. Original western blots of p-cofilin and t-cofilin that were used to produce Figure 6. The inclusion of original blots is required by many scientific journals to ensure data integrity.

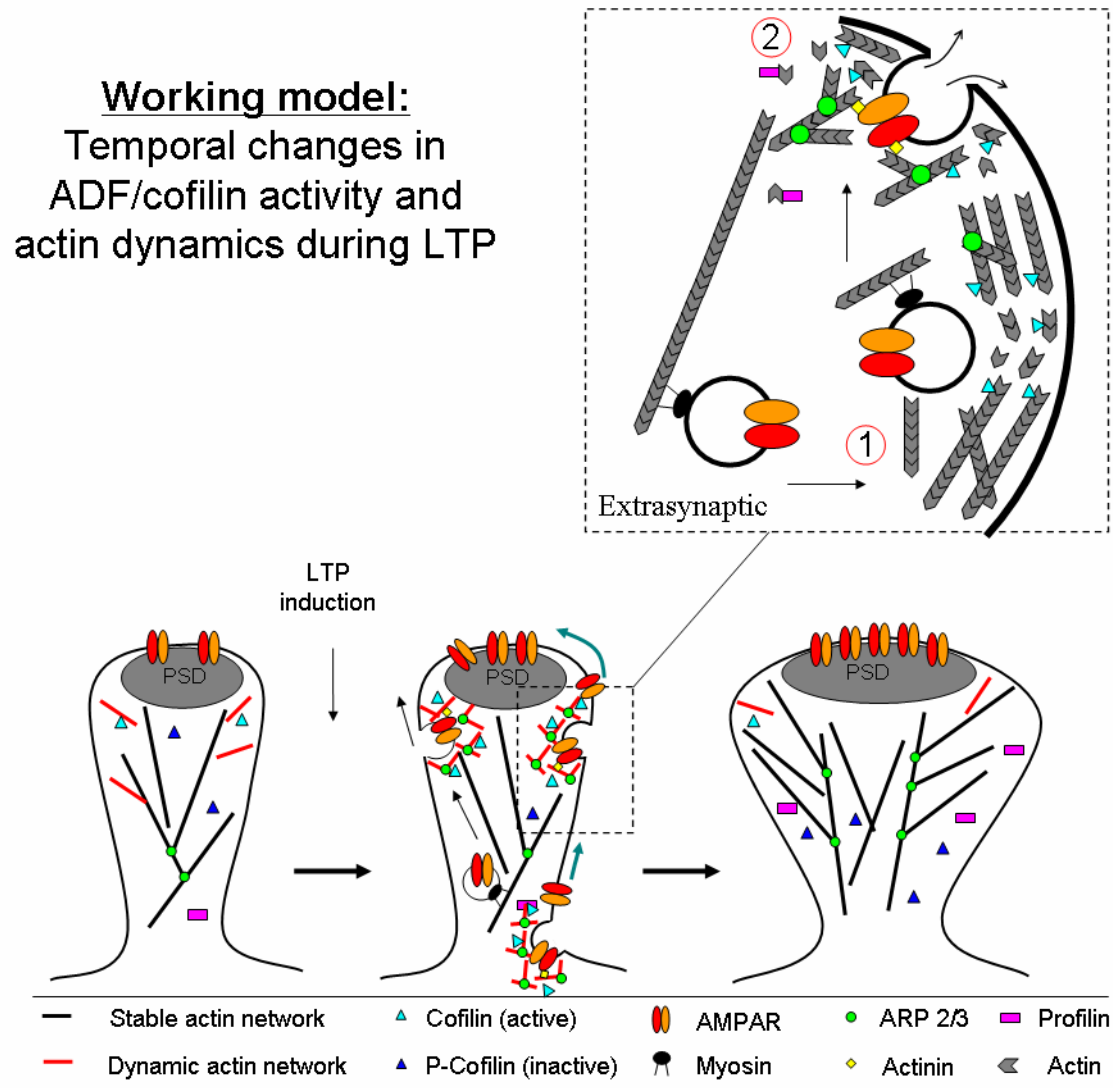

Supplemental figure 8. A schematic diagram showing the temporal model for ADF/cofilin-mediated actin dynamics in regulation of receptor insertion and spine enlargement during LTP. Based on the previous studies, a stable core and a dynamic peripheral of the actin cytoskeleton is presented in the spine. Shortly after LTP induction, the ADF/cofilin activity is upregulated to increase actin dynamics to facilitate receptor insertion. It is plausible that increased ADF/cofilin activity is restricted to the extrasynaptic regions (inside and/or outside the spine) for AMPAR insertion, followed by lateral movement of the receptors into synapse (indicated by blue arrows). Myosin-based vesicle trafficking occurs on stable actin filaments for delivering receptor vesicles to the insertion sites. Later, the ADF/cofilin becomes phosphorylated (activated) to decrease actin dynamics, allowing the expansion of the actin network, leading to enlarged spine, PSD size and receptor stabilization. Other actin-associated proteins, such as Arp2/3 and profilin, could be involved in these actin events in spines. The enlarged region depicts the possible mechanisms underlying the regulation of AMPAR insertion by ADF/cofilin-mediated actin dynamics. ADF/cofilin severing of the existing actin filaments could be responsible (1) for disrupting the "physical barrier" of the actin cortex and (2) for generating new barbed ends for actin assembly to facilitate/drive vesicle fusion to the plasma membrane.

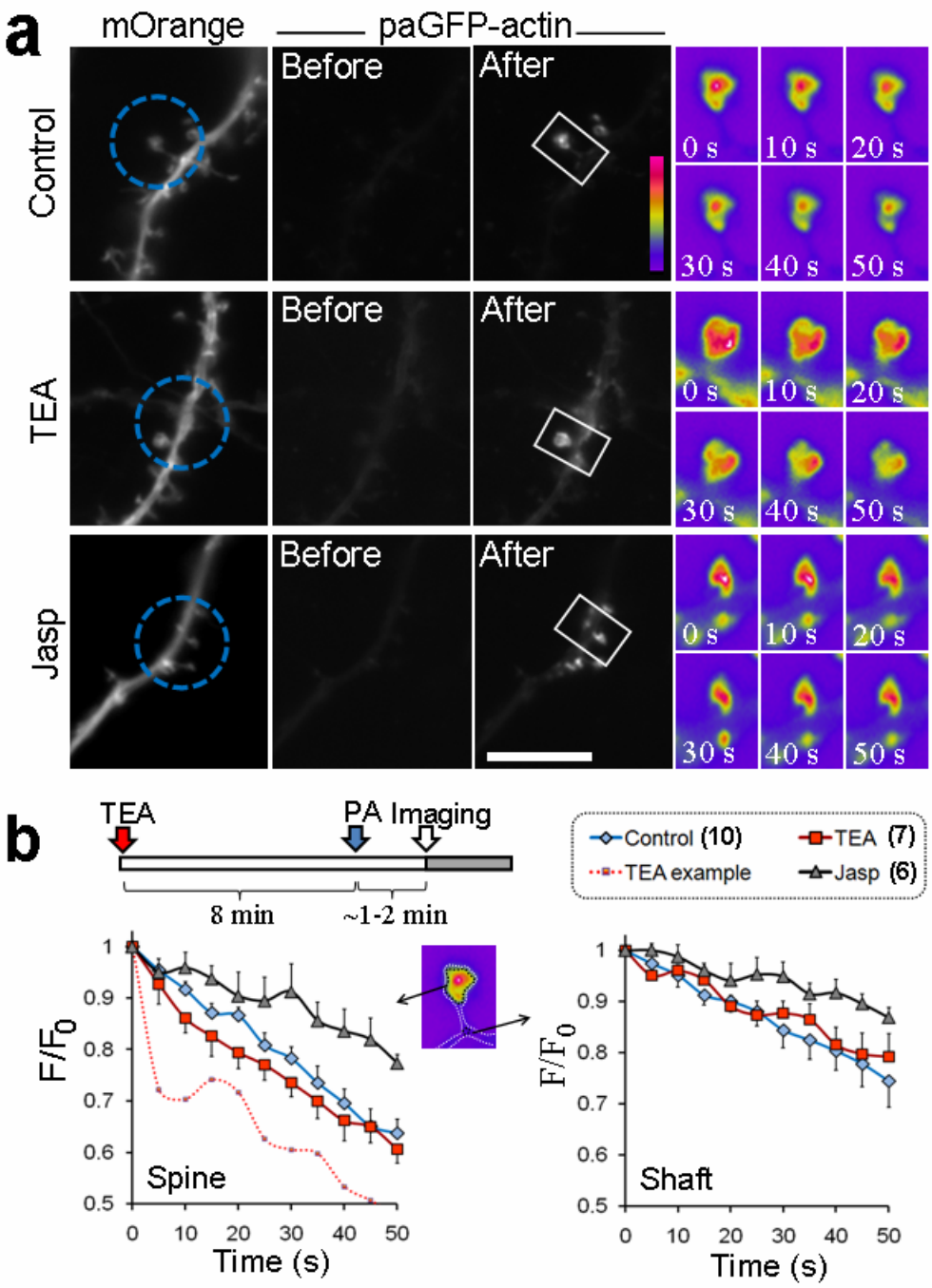

Supplemental figure 9. Changes in photoactivated paGFP-actin fluorescence in spines during TEA-cLTP. (**a**) Representative sets of images showing the change of paGFP-actin fluorescence intensity in dendritic spines under different treatments. The dendritic region containing a spine structure was identified by mOrange fluorescence signals for local photoactivation (blue dotted circles) by UV light. Time-lapse sequences of paGFP-actin fluorescence intensity at the dendritic spines (boxed regions) were magnified and pseudocolored to depict the differential turnover rates of activated paGFP-actin signals in TEA- or Jasplaskinolide (Jasp)-treated neurons. Scale bar: 10 μm. (**b**) A schematic diagram showing the experimental procedures on the UV photoactivation and the time-lapse imaging. Quantification is plotted to show the change of paGFP fluorescence (F/F_0) in dendritic spines and shafts under different treatments. The red dotted line represents a particular spine example, in which

the paGFP-actin fluorescence exhibited a marked decline. While the paGFP-actin fluorescence appeared to decline slightly faster than the control group, it should be noted that no statistical significance was observed between these two groups. It should also be noted that the fluorescence decay of photoactivated paGFP in spines depends on exchange with the cytosol outside the spines (Honkura et al., Neuron 57:719, 2008). Importantly, it was reported that the spine neck poses as a diffusion barrier in an activity-dependent manner (Bloodgood BL & Sabatini B L Science 310, 866–869, 2005). Therefore, this paGFP-actin photoactivation and imaging during cLTP approach does not directly reveal the actin dynamics in the spines. Future experiments employing other imaging techniques (e.g. FRET-based imaging of F-actin/G-actin ratio, Nature Neuroscience 7, 1104 – 1112, 2004) may provide definite answers to the actin dynamics associated synaptic plasticity.